Molecular Dynamics Simulation Study. J. Phys. Chem. B 2010, 114 (47), 15590–15597.

- (19) Tielrooij, K. J.; Garcia-Araez, N.; Bonn, M.; Bakker, H. J. Cooperativity in Ion Hydration. *Science* **2010**, 328 (5981), 1006–1009
- (20) Luo, G. M.; Bu, W.; Mihaylov, M.; Kuzmenko, I.; Schlossman, M. L.; Soderholm, L. X-ray Reflectivity Reveals a Nonmonotonic Ion-Density Profile Perpendicular to the Surface of ErCl3 Aqueous Solutions. *J. Phys. Chem. C* **2013**, *117* (37), 19082–19090.
- (21) Bera, M. K.; Luo, G. M.; Schlossman, M. L.; Soderholm, L.; Lee, S.; Antonio, M. R. Erbium(III) Coordination at the Surface of an Aqueous Electrolyte. *J. Phys. Chem. B* **2015**, *119* (28), 8734–8745.
- (22) Bu, W.; Yu, H.; Luo, G. M.; Bera, M. K.; Hou, B. Y.; Schuman, A. W.; Lin, B. H.; Meron, M.; Kuzmenko, I.; Antonio, M. R.; Soderholm, L.; Schlossman, M. L. Observation of a Rare Earth Ion-Extractant Complex Arrested at the Oil Water Interface During Solvent Extraction. J. Phys. Chem. B 2014, 118 (36), 10662–10674.
- (23) Meron, M.; Gebhardt, J.; Brewer, H.; Viccaro, J. P.; Lin, B. Following transient phases at the air/water interface. *Eur. Phys. J.: Spec. Top.* **2009**, *167*, 137–142.
- (24) Miller, M.; Chu, M. Q.; Lin, B. H.; Meron, M.; Dutta, P. Observation of Ordered Structures in Counterion Layers near Wet Charged Surfaces: A Potential Mechanism for Charge Inversion. *Langmuir* **2016**, 32 (1), 73–77.
- (25) Woodward, J. T.; Ulman, A.; Schwartz, D. K. Self-assembled monolayer growth of octadecylphosphonic acid on mica. *Langmuir* **1996**, *12* (15), 3626–3629.
- (26) Kmetko, J.; Datta, A.; Evmenenko, G.; Durbin, M. K.; Richter, A. G.; Dutta, P. Ordering in the subphase of a langmuir monolayer: X-ray diffraction and anomalous scattering studies. *Langmuir* **2001**, *17* (16), 4697–4700.
- (27) Kmetko, J.; Datta, A.; Evmenenko, G.; Dutta, P. The effects of divalent ions on Langmuir monolayer and subphase structure: A grazing-incidence diffraction and Bragg rod study. *J. Phys. Chem. B* **2001**, *105* (44), 10818–10825.
- (28) Dupres, V.; Cantin, S.; Benhabib, F.; Perrot, F.; Fontaine, P.; Goldmann, M.; Daillant, J.; Konovalov, O. Superlattice formation in fatty acid monolayers on a divalent ion subphase: Role of chain length, temperature, and subphase concentration. *Langmuir* **2003**, *19* (26), 10808–10815.
- (29) Kaganer, V. M.; Mohwald, H.; Dutta, P. Structure and phase transitions in Langmuir monolayers. *Rev. Mod. Phys.* **1999**, *71* (3), 779–819.
- (30) Leveiller, F.; Jacquemain, D.; Lahav, M.; Leiserowitz, L.; Deutsch, M.; Kjaer, K.; Alsnielsen, J. Crystallinity of the Double-Layer of Cadmium Arachidate Films at the Water-Surface. *Science* **1991**, 252 (5012), 1532–1536.

commensurate ionic superlattices, although their detailed structures differ because the floating monolayers pack differently. The incommensurate lattices seen with HA/light (Figure Sc), HA/heavy (Figure 5d) and DHDP/heavy (Figure 5f) are very close in dimensions, although again there are quantitative differences that are much larger than the resolution of the X-ray diffraction technique. A doubling of the lattice parameters for the incommensurate lattice seen with ODPA/heavy (Figure 5b) is also quite close to the other heavy ion lattices. It is possible that the larger lattices actually have four ions within their unit cells that cannot be detected. Since so few peaks are observable, a full model of the unit cell cannot be developed accurately. These similarities are driven by factors yet to be determined.

Returning to the Z-dependence, it is striking that light and heavy structures are both perfectly independent of Z, with the transition happening over a narrow Z range. Although there is an intermediate region with no structure, the transition is somewhat reminiscent of a first order structural phase transition, because it is much sharper than the reported slow trends in coordination number. ^{14–16} It is possible that the coordination number in a relatively dense layer at the surface is quite different from the bulk coordination number, with the unit cell size serving as the only available indication of the interfacial coordination number. Alternatively, as with phase transitions, it is possible that a continuous change in a relevant parameter (such as hard ionic core size) drives a sharp change in the structure. Further characterization is necessary to distinguish between these possibilities or identify other mechanisms not yet considered.

CONCLUSION

The ordering induced in dilute lanthanide solutions near floating Langmuir monolayers of several different molecules was probed with GIXD. These studies show that counterions can order near interfaces in a variety of ways, driven by the delicate interplay of subtle and poorly identified factors. The lattices observed were independent of changing Z until a threshold was reached which caused the structure to change suddenly, despite the well-known, continuous decrease in atomic size of the lanthanide series. This behavior was consistently observed with several different Langmuir monolayers of different headgroup type and chain length. The formation of different structures, with different properties, may help explain some of the differences seen in the behavior of different lanthanides, such as the varying efficiencies for liquidliquid extraction. These structures may also give some insight into the hydration behavior of lanthanides, especially near interfaces.

AUTHOR INFORMATION

Corresponding Author

*E-mail: pdutta@northwestern.edu.

ORCID

Mitchell Miller: 0000-0001-7266-1092 Binhua Lin: 0000-0001-5932-4905 Pulak Dutta: 0000-0002-2111-0546

Author Contributions

The manuscript was written through contributions of all authors. All authors have given approval to the final version of the manuscript.

Notes

The authors declare no competing financial interest.

ACKNOWLEDGMENTS

This work was supported by the US National Science Foundation under Grant No. DMR-1612876. The X-ray diffraction measurements were performed at ChemMatCARS (Sector 15, Advanced Photon Source). ChemMatCARS is supported by the U.S. National Science Foundation under Grant NSF/CHE-1346572. The Advanced Photon Source is supported by the U.S. Department of Energy under Contract DE-AC02-06CH11357.

REFERENCES

- (1) Kenyon, A. J. Recent developments in rare-earth doped materials for optoelectronics. *Prog. Quantum Electron.* **2002**, *26* (4–5), 225–284
- (2) Wang, G. F.; Peng, Q.; Li, Y. D. Lanthanide-Doped Nanocrystals: Synthesis, Optical-Magnetic Properties, and Applications. *Acc. Chem. Res.* **2011**, *44* (5), 322–332.
- (3) White, R. L. Review of Recent Work on Magnetic and Spectroscopic Properties of Rare-Earth Orthoferrites. *J. Appl. Phys.* **1969**, *40* (3), 1061–1069.
- (4) Zaleski, C. M.; Depperman, E. C.; Kampf, J. W.; Kirk, M. L.; Pecoraro, V. L. Synthesis, structure, and magnetic properties of a large lanthanide-transition-metal single-molecule magnet. *Angew. Chem., Int. Ed.* **2004**, *43* (30), 3912–3914.
- (5) Molander, G. A.; Romero, J. A. C. Lanthanocene catalysts in selective organic synthesis. *Chem. Rev.* **2002**, *102* (6), 2161–2185.
- (6) Xie, F.; Zhang, T. A.; Dreisinger, D.; Doyle, F. A critical review on solvent extraction of rare earths from aqueous solutions. *Miner. Eng.* **2014**, *56*, 10–28.
- (7) Gschneidner, K. A.; Eyring, L.; Lander, G. H. Handbook on the Physics and Chemistry of Rare Earths; Elsevier: Oxford, 2002; Vol. 32.
- (8) Siekierski, S. The Itinerant Character of 4f Orbitals in Lanthanide Metals by a Comparison of Lanthanide Contraction in Metals and Ionic Compounds. *Inorg. Chim. Acta* 1985, 109 (3), 199–201.
- (9) D'Angelo, P.; Spezia, R. Hydration of Lanthanoids(III) and Actinoids(III): An Experimental/Theoretical Saga. *Chem. Eur. J.* **2012**, *18* (36), 11162–11178.
- (10) Richens, D. T. The Chemistry of Aqua Ions: Synthesis, Structure and Reactivity: A Tour Through the Periodic Table of the Elements. Wiley: Chichester, U.K., 1997.
- (11) Ferru, G.; Reinhart, B.; Bera, M. K.; Olvera de la Cruz, M.; Qiao, B.; Ellis, R. J. The Lanthanide Contraction beyond Coordination Chemistry. *Chem. Eur. J.* **2016**, 22 (20), 6899–6904.
- (12) Dam, H. H.; Reinhoudt, D. N.; Verboom, W. Multicoordinate ligands for actinide/lanthanide separations. *Chem. Soc. Rev.* **2007**, *36* (2), 367–377.
- (13) Rizkalla, E. N.; Choppin, G. R. Hydration of Lanthanides and Actinides in Solution. *J. Alloys Compd.* **1992**, *180*, 325–336.
- (14) Duvail, M.; Spezia, R.; Vitorge, P. A dynamic model to explain hydration behaviour along the lanthanide series. *ChemPhysChem* **2008**, 9 (5), 693–696.
- (15) Allen, P. G.; Bucher, J. J.; Shuh, D. K.; Edelstein, N. M.; Craig, I. Coordination chemistry of trivalent lanthanide and actinide ions in dilute and concentrated chloride solutions. *Inorg. Chem.* **2000**, *39* (3), 595–601.
- (16) Habenschuss, A.; Spedding, F. H. The Coordination (Hydration) of Rare-Earth Ions in Aqueous Chloride Solutions from X-Ray-Diffraction 0.3. Smcl3, Eucl3, and Series Behavior. *J. Chem. Phys.* **1980**, 73 (1), 442–450.
- (17) Zhang, J.; Heinz, N.; Dolg, M. Understanding Lanthanoid(III) Hydration Structure and Kinetics by Insights from Energies and Wave functions. *Inorg. Chem.* **2014**, 53 (14), 7700–7708.
- (18) Beuchat, C.; Hagberg, D.; Spezia, R.; Gagliardi, L. Hydration of Lanthanide Chloride Salts: A Quantum Chemical and Classical

Table 1. Summary of Observed Lattices in Terms of Monolayer Material and Lanthanide Atomic Numbers

	"light" lanthanides	intermediate lanthanides (no ionic lattice)	"heavy" lanthanides
ODPA	Z = 58-62	Z = 63-65	Z = 66-70
	(Figure 5a) commensurate $a = b = 17.1 \text{ Å}$ $\gamma = 60^{\circ}$		(Figure 5b) commensurate $a=10.28$ Å $b=10.0$ Å $\gamma=66.93^\circ$ incommensurate $a=6.77$ Å $b=5.31$ Å $\gamma=79.28^\circ$
HA	Z = 58-60	Z = 62	Z = 63-70
	(Figure 5c) incommensurate $a = 13.82$ Å $b = 14.15$ Å $\gamma = 61.2^{\circ}$		(Figure 5d) commensurate $a=9.90$ Å $b=8.26$ Å $\gamma=69^\circ$ incommensurate $a=b=13.46$ Å $\gamma=60^\circ$
DHDP	Z = 57-64		Z = 65-70
	(Figure 5e) no ionic lattice		(Figure 5f) incommensurate $a = b = 14.2 \text{ Å} \gamma = 60^{\circ}$

structure with a = 9.90 Å, b = 8.26 Å, and $\gamma = 69^{\circ}$ and an incommensurate structure with a = b = 13.46 Å and $\gamma = 60^{\circ}$.

Dihexadecylphosphate (DHDP). DHDP, the final molecule used, is a double-chain phosphate. It shows the weakest ionic ordering. For the light class of ions, La^{3+} , Ce^{3+} , Pr^{3+} , Nd^{3+} , Sm^{3+} , Eu^{3+} , and Gd^{3+} (Z=57 to 64), no ionic structure at all was detected. Only a single molecular monolayer peak is observed, corresponding to a hexagonal lattice with a=b=4.76 Å and $\gamma=60.0^{\circ}$ (Figure 4b). The rod scan of this peak indicates a thickness of 20 Å.

We have previously reported that an incommensurate ionic lattice is generated by the heavy lanthanide Er^{3+} beneath a DHDP monolayer²⁴ (Figure 4a). The present study adds Tb^{3+} , Dy^{3+} , and Yb^{3+} (Z=65 to 70) to the ions that form the same structure (Figure 4a). The DHDP monolayer forms an oblique structure with a=4.59 Å b=6.24 Å and $\gamma=42.6^{\circ}$ and an incommensurate ionic structure with a=b=14.2 Å and $\gamma=60^{\circ}$.

DISCUSSION

These results show an unexpected variety of structures (see Table 1 and Figure 5), both commensurate and incommensurate, with a large range of spacings. Of course, counterion lattices under floating monolayers have been reported before: Cd $^{2+,30}$ Pb $^{2+,26}$ Mg $^{2+,27,28}$ Mn $^{2+,27,28}$ show commensurate structures with large supercells, and each element forms a different structure. While these structures form only in the presence of ions, the detailed chemical composition of any of these large unit cells has never been established, and why they are so large has not been explained. Even the charge accounting is not well understood; the unequal distribution of positive ions and negative headgroups is typically ignored when describing the unit cells. Of course, they are quite reasonably thought to contain water molecules (which are almost invisible to X-rays) in addition to one or more metal ions. (X-ray scattering determines the lattice structure, and rod scans indicate that the ionic lattice comes from a very thin monolayer, but it does not tell us how many ions are present per repeat unit.) The lattice spacings reported in this paper are also large compared to the size of the bare ions. What is different in these results is that (a) the ionic lattices can be incommensurate in multiple cases, and in these cases the structures are not imposed by chemical bonds with the molecular structure above it, but rather are determined by lateral interactions between ions;²⁴ and (b) even with apparently very similar ions (lanthanides), we see quite different structures being formed by different lanthanides under the same floating monolayer.

One factor determining the structures formed is the headgroup of the molecular monolayer, which presumably affects the areal density of lanthanides in the monolayer through the degree of dissociation (i.e., the charge of the

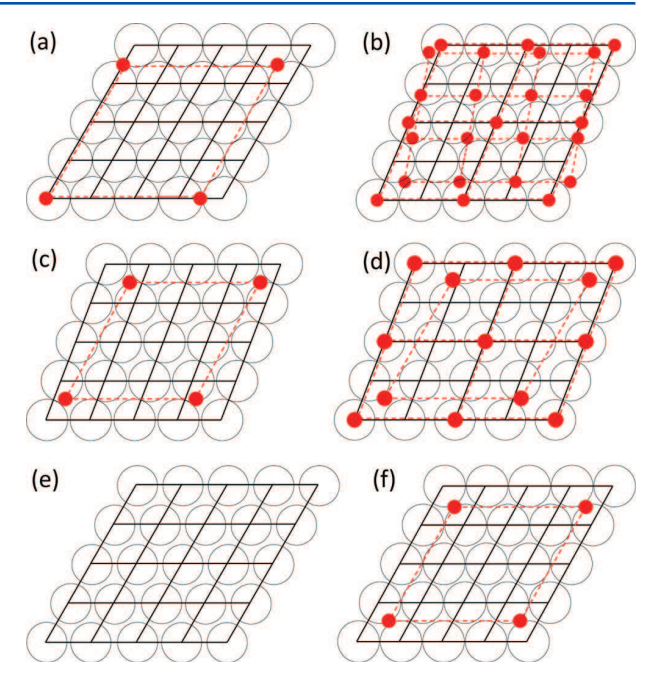


Figure 5. Real-space lattice depictions of structures formed in (a) ODPA with light lanthanides, (b) ODPA with heavy lanthanides, (c) HA with light lanthanides, (d) HA with heavy lanthanides, (e) DHDP with light lanthanides, and (f) DHDP with heavy lanthanides. Black circles represent cross sections of hydrocarbon chains in the monolayer, and solid black lines indicate the chain lattice. Dotted red lines and red circles show the ionic lattices; note, however, that the number of lanthanide ions in a unit cell is not known, and therefore the red circles are not necessarily the only lanthanide ions in the unit cell. The two types of lines coincide when the structures are commensurate. The relative locations of the lattices present in a given system (and the orientations, when there are incommensurate lattices) is arbitrary because X-ray scattering does not provide this information.

monolayer), and also helps determine the degree of ordering and whether it is commensurate. The other factor is the atomic number of the lanthanide. The form of the dependence on Z is unexpected. We observe entirely different lattices for heavy and light lanthanides with the same molecular monolayer, with no variation in the peak positions within the heavy or light class. The transition between the light and heavy structure in DHDP and HA happens at slightly different values of Z, and the intermediate region where there is no observed structure is also slightly different (Table 1). However, both transitions happen in the range where there is reported to be a rapid but continuous change in the coordination number. 14–16

There are some common features. Both ODPA/heavy (Figure 5b) and HA/heavy (Figure 5d) show 2 × 2

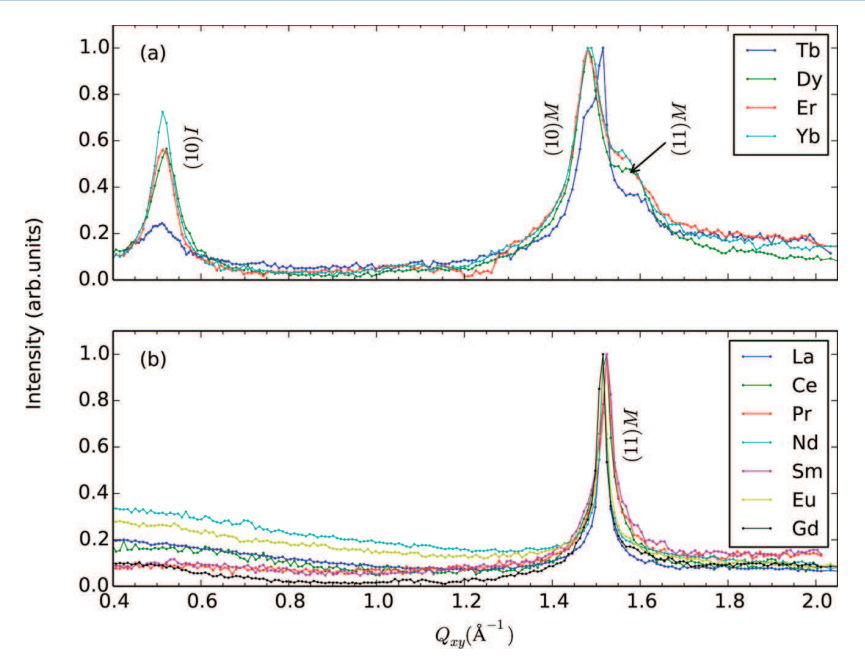


Figure 4. Z-integrated ($Q_Z = 0 \text{ Å}^{-1}$ to 0.6 Å^{-1}) GIXD data from heavy (a) and light (b) lanthanides under a floating DHDP monolayer. Each peak is indexed according to structures described in the text with M = molecular monolayer and I = incommensurate ionic lattice.

an oblique cell with a=5.14 Å, b=5.0 Å and $\gamma=66.93^\circ$. The remaining peaks all have very broad intensities along the Q_Z axis, indicating an ionic layer; however, some show minor oscillations in intensity. This oscillation is generally accepted to originate from a slight variation in the vertical position of the ions. ^{27,28} Three of the peaks (labeled with C for commensurate) can be indexed by half integers of the molecular lattice, showing there is again a commensurate ionic supercell with a=10.28 Å b=10.0 Å and $\gamma=66.93^\circ$. The remaining peaks (labeled I for incommensurate) cannot be indexed to any commensurate lattice, but can be indexed as originating from an incommensurate lattice with a=6.77 Å b=5.31 Å and $\gamma=79.28^\circ$. It should be noted that we cannot tell whether these ionic structures coexist with one another or are divided into separate domains.

Heneicosanoic Acid (HA). Lanthanide ions under HA once again show two different structures for light and heavy lanthanides. An ionic lattice was observed with light lanthanides Ce^{3+} , Pr^{3+} , and Nd^{3+} (Z=58 to 60) in the subphase. A different ionic lattice was detected using subphases of heavy lanthanides, Eu^{3+} , Gd^{3+} , Tb^{3+} , Dy^{3+} , Er^{3+} , and Yb^{3+} (Z=63 to 70). No structure was seen in solutions of La^{3+} (Z=57) or Sm^{3+} (Z=62)

Diffraction results from both light and heavy lanthanides with a HA monolayer are somewhat more difficult to interpret (Figure 3b). These systems show a unique time dependence: after a very short time of X-ray exposure (less than 1 min), the complex ion and monolayer structure transitions to a simple, one peak monolayer structure. In some scans, this "long-time" monolayer structure even begins to develop within the first 10 s snapshot. These long time peaks can be seen in some of our data, but are unlabeled and unindexed. The time-dependent behavior is not reversible and only occurs in the region of direct X-ray exposure; moving the sample to scan a region that has not been previously exposed shows the same structure as an entirely fresh sample. This behavior is observed in the presence of both light and heavy type lanthanides. It should be noted

that this phenomenon is distinct from commonly observed radiation damage. The structure of the floating monolayer is changed but not destroyed in this short time, while the ionic structure is removed. Only after the sample has been exposed to X-rays for 30 min or more is the more familiar type of beam damage (loss of monolayer peaks) observed. Also note that the diffraction peaks used in this paper to determine lattice structures are the ones seen at early times (before any kind of radiation damage).

The three monolayer peaks that come from the initial monolayer structure with light lanthanides (that vanish with time) are labeled with M in Figure 3b. The undamaged monolayer structure is an oblique unit cell with a = 4.66 Å, b =4.43 Å, and $\gamma = 69.18^{\circ}$. The rod scan profiles indicate a layer thickness of 25 Å, consistent with the length of a HA molecule.²⁶ The ionic structure is incommensurate with the floating monolayer lattice: an oblique unit cell with a = 13.82 Å, b = 14.15 Å, and $\gamma = 61.2^{\circ}$ (labeled with an *I* in Figure 3b). The independence of the monolayer and ionic lattices is significant because the lateral ordering of the ions is not being driven by the monolayer structure but rather by ion-ion interactions. Further discussion of this can be found in ref 24. The final monolayer structure (observed after <400 s of X-ray exposure) is a hexagonal lattice with a = b = 4.86 Å and $\gamma = 60.0^{\circ}$. This structure is the same as a HA monolayer floating on pure water at room temperature, ²⁹ despite the measurements being taken at 7.5 $^{\circ}\text{C}$. In this paper we do not consider the radiationdamaged structure further.

We have previously reported both a commensurate and incommensurate ionic structure composed of the heavy lanthanide Er^{3+} beneath a floating HA monolayer.²⁴ We expand upon those results, adding Eu^{3+} , Gd^{3+} , and Tb^{3+} to the previously observed elements. These data are shown in Figure 3a. The peak positions, and thus the lattices formed, are the same in all cases although the peak intensities vary. The HA monolayer structure has the following parameters: a = 4.95 Å, b = 4.13 Å, and $\gamma = 69^{\circ}$. There is also a commensurate ionic

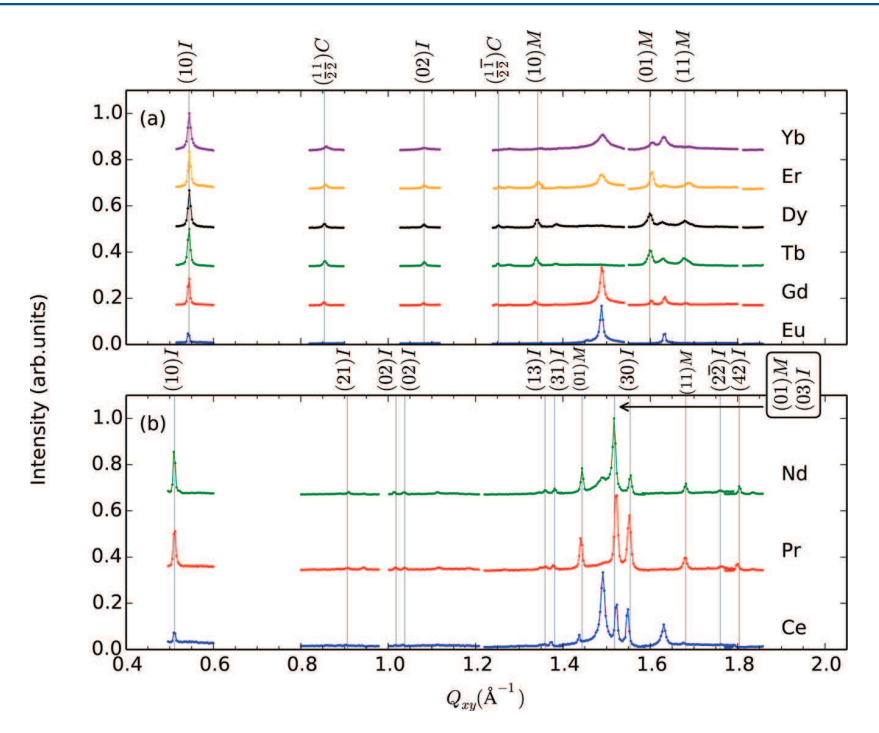


Figure 3. Z-integrated ($Q_Z = 0 \text{ Å}^{-1}$ to 0.6 Å⁻¹) GIXD data from heavy (a) and light (b) lanthanides under a floating HA monolayer. Each peak is indexed according to structures described in the text with M = molecular monolayer, C = commensurate ionic lattice, and I = incommensurate ionic lattice. The separations between scan areas is due to the scanning method used to reduce radiation damage of the ionic lattices. Note the unlabeled peaks at $Q_{XY} = 1.49 \text{ Å}^{-1}$ and 1.62 Å⁻¹ come from the "long-time" (radiation-damaged) molecular monolayer structure.

RESULTS

GIXD is a technique that probes ordering very close to an interface. We collect scattering intensity as a function of inplane (Q_{xy}) and normal-to-plane (Q_z) components of Q, the scattering vector. Because the monolayer is a powder in the plane, it is not possible to distinguish the x- and y-components of the scattering vector. The positions and widths of the measured peaks indicate the structure(s) within our samples. Because the intensities are distributed along vertical rods and not rings, the scattering must originate from thin horizontal layers. The width of a peak in the Q_Z direction is inversely proportional to the thickness of these layers and can thus be used to identify the layer. In a previous paper²⁴ we have presented data on Er3+ ions under HA and DHDP monolayers, showing "rod scans" (scans in the Q_Z direction) and explained how these scans tell us which diffraction peaks are from the monolayer and which are from ionic lattices. In this paper, the same identification method is used, but only the in-plane (Q_{xy}) scans are shown.

Octadecylphosphonic Acid (ODPA). OPDA has a single saturated chain with a phosphonic acid headgroup. We studied ODPA monolayers spread on 10^{-4} M solutions containing La³⁺ (Z = 57), Ce³⁺ (Z = 58), Pr³⁺ (Z = 59), Nd³⁺ (Z = 60), Sm³⁺ (Z = 62), Eu³⁺ (Z = 63), Gd³⁺ (Z = 64), Tb³⁺ (Z = 65), Dy³⁺ (Z = 66), Er³⁺ (Z = 68), and Yb³⁺ (Z = 70). We detected no ionic ordering in subphases containing La³⁺ at the low-Z end of the lanthanide series and Eu³⁺, Gd³⁺, and Tb³⁺ in the middle. With the other ions we observed two different ionic structures depending on whether the ion was "light" or "heavy". The light structure was observed using solutions of Ce³⁺, Pr³⁺, Nd³⁺, and Sm³⁺ (Z = 58 to E = 66 t

For the light class of ions, three peaks were identified in the scattering data. Two peaks have the same Q_{XY} value but different Qz values (labeled (10)M and (11)M in Figure 2b), indicating a tilt in the molecules with respect to the surface normal. From the widths of their rod scans along the Q_Z axis, we determine that these peaks originate from a layer approximately 25 Å thick, which is consistent with the length of an ODPA molecule. 25 We can also determine the in-plane ordering from the Q_{XY} positions of these peaks. The ODPA molecules form a hexagonal lattice with a = b = 4.89 Å and $\gamma =$ 60°. The third peak has a notably different profile (labeled (10) C in Figure 2b). The rod scan of this peak shows nearly uniform intensity along the entire detector region, indicating a very thin layer. We estimate the thickness of this layer to be < \approx 6 Å, which is comparable to the size of the lighter lanthanide ions (~2 Å) plus the capillary roughness of the water surface (~3 Å). Since there is only one first-order peak present from this structure, it can be indexed as originating from a hexagonal lattice with a = b = 17.1 Å and $\gamma = 60^{\circ}$. This is a 3.5-fold multiple in both the a and b direction of the molecular lattice. Thus, the ionic lattice is a supercell of the molecular lattice, i.e., the two lattices are commensurate. Large, ionic supercells have been observed with many divalent ions 26-28 but rarely with trivalent ions.²⁴ It should be noted that we do not know how many lanthanide ions are contained in each supercell; however, the large size of the supercell indicates that the ionic structure is not formed by bare ions alone but by larger units, presumably hydrated complexes.

The diffraction pattern created from heavy lanthanides is more complicated (Figure 2a). Three peaks can be assigned to a thick molecular layer from their rod scans. As with the light lanthanides, the peak widths of these rod scans indicate a layer that is 25 Å thick. The molecular lattice for heavy lanthanides is

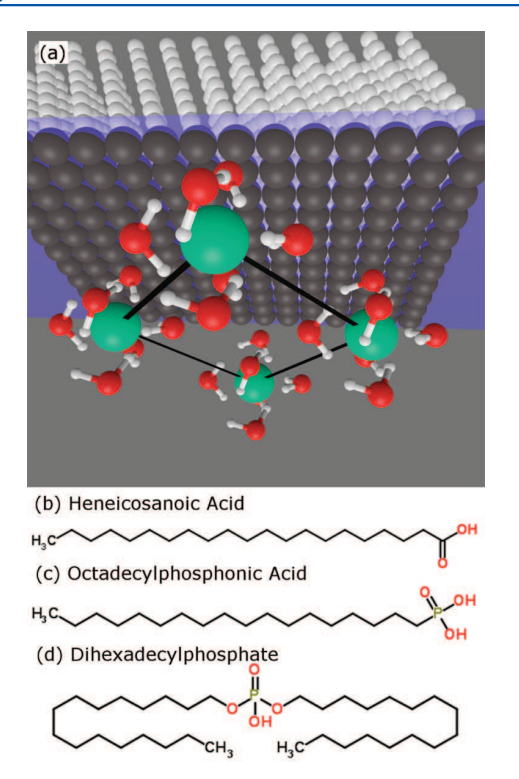


Figure 1. (a) Schematic diagram of the system studied, seen from below (within the water subphase). The floating molecules are represented by the black head groups and white hydrocarbon tails. The green lanthanide ions are surrounded by red and white water molecules. The three monolayer-forming molecules used in the present studies are (b) HA, (c) ODPA, and (d) DHDP.

Monolayer materials were dissolved in chloroform or a 9:1 mixture of hexane and ethanol depending on the material's solubility. Heneicosanoic acid (HA, > 99%), dihexadecylphosphate (DHDP, no purity listed), and octadecylphosphonic acid (ODPA, 97%) were all purchased from Sigma-Aldrich. These molecules were chosen for the commonalities their headgroups share with modern industrial solvent extractants. HA and DHDP were dissolved in chloroform (>99.99%, Fisher Chemicals) at room temperature to a concentration of 1 mM. ODPA was dissolved in a 9:1 mixture of hexane (98.5%, BDH Chemicals) and ethanol (200 proof, Koptec) to a concentration of 1 mM.

Grazing Incidence X-ray Diffraction (GIXD). All X-ray measurements were conducted at the Advanced Photon Source (Argonne National Laboratory) on beamline 15-ID with 10 keV X-rays. Approximately 300 mL of electrolyte solution were poured into a Teflon Langmuir trough. An integrated chilling system was used to maintain a sample temperature of 7.5 °C. After the sample temperature was allowed to stabilize, a precise amount of monolayer solution was spread dropwise over the liquid surface with a microliter syringe. A Wilhelmy plate made of chromatography paper was used to measure and maintain a specific surface pressure during GIXD measurements

The liquid surface was illuminated with X-rays at an incident angle of 0.09° to the horizontal plane, which is 80% of the critical angle for total external reflection. Scattered X-rays were collected with a Pilatus 100 K area detector in pinhole geometry. Samples with DHDP and ODPA monolayers were scanned continuously over a large angular region ($Q_{xy} = 0.3 \text{ Å}^{-1}$ to $Q_{xy} = 2.6 \text{ Å}^{-1}$) with electronic slits 3 pixels wide and patching the resulting series images. HA samples were scanned in a different mode due to their unique time-dependent behavior (discussed later in this paper). For HA, a first scan was performed to locate the diffraction peaks; then the detector was moved directly to the observed peak locations, and 40 ten-second-long exposures were recorded with the trough moved laterally to expose a fresh spot on the surface for each peak.

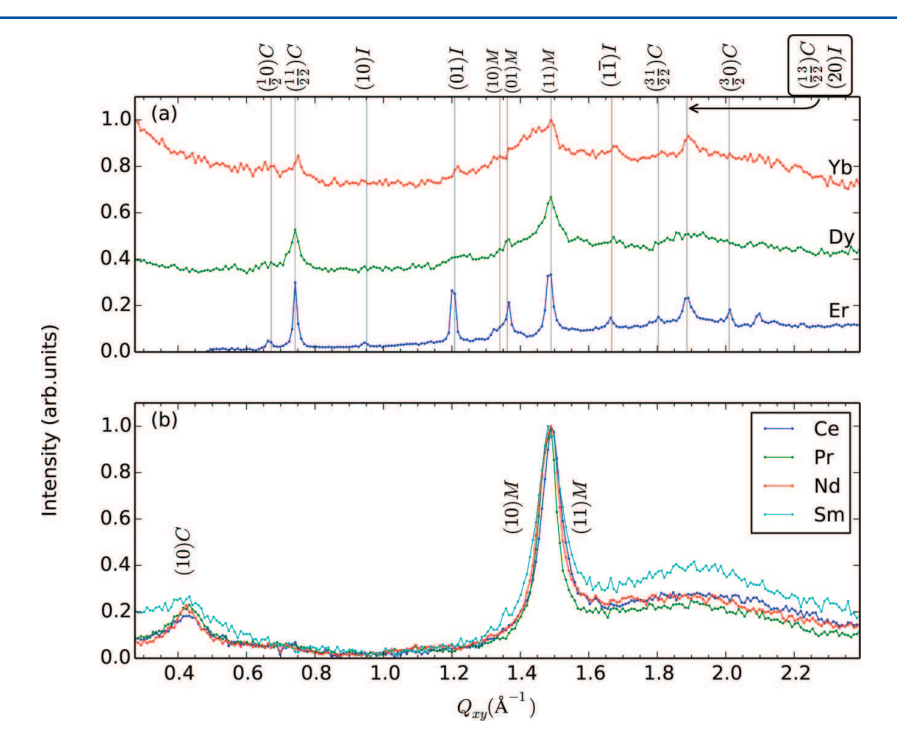


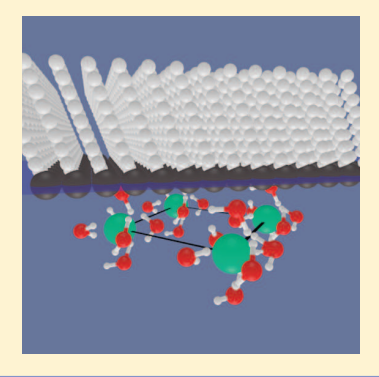
Figure 2. Z-integrated ($Q_Z = 0 \text{ Å}^{-1}$ to 0.6 Å^{-1}) GIXD data from heavy (a) and light (b) lanthanides under a floating ODPA monolayer. Each peak is indexed according to structures described in the text with M = molecular monolayer, C = commensurate ionic lattice, and I = incommensurate ionic lattice.

pubsiacs.org/Langmuir

Atomic Number Dependent "Structural Transitions" in Ordered Lanthanide Monolayers: Role of the Hydration Shell

Mitchell Miller, † Miaoqi Chu, † Binhua Lin, ‡ Wei Bu, ‡ and Pulak Dutta*, †

ABSTRACT: When lanthanide ions are present in the aqueous subphase of a floating monolayer (Langmuir film), the ions attracted to the interface will in many cases form commensurate and/or incommensurate two-dimensional structures. These lattices depend not only on the molecules forming the monolayer, but also on the atomic number of the lanthanide, with a sudden change between the lattice formed by lighter ions and that formed by heavier ions under a given monolayer. Since there are few other relevant differences between the lanthanides, we attribute the Z-dependent "transition" to the number of water molecules associated with each ion. The first hydration shell is thought to vary continuously from ~9 in lighter lanthanides to ~8 in heavier lanthanides.



■ INTRODUCTION

Studying the complexation and hydration properties of metal ions is crucial to understanding their solubilities and transport behaviors. The lanthanide series in particular has been the focus of much modern study due to their enormous range of applications and the importance of rare earths for modern electronic, optical, and magnetic^{3,4} systems as well as catalysis.⁵ In principle, all lanthanides should be chemically and physically quite similar; in practice, there are significant differences, for example, in the efficiency of extraction processes.

Lanthanide coordination behavior is generally understood to be driven by the "lanthanide contraction," the small but significant decrease in atomic radius as the atomic number (Z) increases across the lanthanide series.^{7,8} This size decrease manifests itself as a change in coordination number, the number of water molecules in the first hydration shell, from 9 to 8.9,10 In addition, it has been seen to have impacts on aggregation behavior beyond the first coordination sphere. 11 The coordination number of these ions is used to explain the physical chemistry of the lanthanides, such as their extraction efficiencies^{6,12} and solvation enthalpy.¹

The transition in coordination number is much more complicated than one might guess. Experimental studies and simulations have shown a continuous change from ~9 water molecules to ~8, but they do not agree about exactly where it happens along the lanthanide series. 14-16 In addition to the change in coordination number, there are also alterations to the shape of the surrounding water molecules. 14,17 Although these complexes are typically treated as independent units, studies indicate that hydrated metal ions have long-range interactions via both water molecules 18 and counterions 19 beyond the first hydration shell. These effects appear to be magnified near interfaces where density oscillations²⁰ and large, multi-ion complexes²¹ form naturally at sufficient concentrations.

The experiments we report here differ from others that have been performed to explore the differences between different lanthanide ions. We have used grazing-incidence X-ray scattering to study lanthanides that are attracted to a charged, floating monolayer and form ordered two-dimensional lattices (Figure 1). We observe unexpected effects that are not continuous changes as a function of the atomic number Z.

It should be noted that this experimental system models a crucial stage of the liquid-liquid extraction procedure with which many rare earths are separated and refined.⁶ During such extraction, extractant molecules move from the bulk of an organic phase to the interface with an ion rich aqueous phase. At this interface, ions bind with extractant molecules and form complex structures which then return to the bulk of the organic phase.²² Our model system probes the ion-extractant interactions at the moment of first contact, in situ.

EXPERIMENTAL SECTION

Sample Preparation. Aqueous solutions of lanthanide salts at 10⁻⁴ M were prepared immediately before all X-ray measurements. Solid lanthanide chloride salts were purchased from Sigma-Aldrich (>99%) (LaCl₃, CeCl₃, PrCl₃, NdCl₃, SmCl₃, EuCl₃, GdCl₃, TbCl₃, DyCl₃, ErCl₃, YbCl₃) and used with no further purification. Salts were then dissolved in prechilled (T = 2 °C to minimize cooling time between samples) ultrapure Millipore water with resistivity 18.2MΩcm. Sample pH was unadjusted (~5.5 due to ambient CO₂) to maintain purity.

Received: December 23, 2016 Revised: January 19, 2017 Published: January 20, 2017

Department of Physics & Astronomy, Northwestern University, Evanston, Illinois 60208, United States [‡]Center for Advanced Radiation Sources, University of Chicago, Chicago, Illinois 60637, United States